PCCP

ROYAL SOCIETY OF CHEMISTRY

PAPER

View Article Online
View Journal | View Issue

Check for updates

Cite this: *Phys. Chem. Chem. Phys.*, 2021, **23**, 14027

Effect of curing reaction types on the structures and properties of acetylene-containing thermosets: towards optimization of curing procedure†

Junli Zhu, Liquan Wang,* Jiaping Lin,* Lei Du and Qixin Zhuang

Received 26th October 2020,
Accepted 1st June 2021

DOI: 10.1039/d0cp05580h

rsc.li/pccp

High-temperature thermosets are usually prepared from resins containing alkynyl groups, and their properties depend much upon the curing process containing various types of curing reactions. However, how the curing process affects the properties remains unclear due to the complicated curing reactions. We used molecular dynamics simulations to investigate the effect of curing reaction types, including cyclotrimerization, Diels–Alder reaction, and radical reaction, on the structures and properties of imide oligomers terminated with alkynyl groups. The results show that the cycloadditions such as cyclotrimerization and Diels–Alder reaction endow the thermosets with rigid structures and high moduli. Compared with the cycloadditions, the radical reaction enables the formation of flexible cured structures, which can enhance the toughness of thermosets. The differences in thermal and mechanical properties caused by different curing types were elucidated by the relaxation processes of fragments in these cured systems and were explained by the variation of torsion energy in different curing forms. As this work aims to optimize the curing procedure to obtain high-performance resins with desired properties, different curing procedures were finally designed according to the theoretical studies, and the obtained cured polymers show significant differences in the properties from different curing ways. The results can guide the preparation of desired thermosetting resins by tuning the curing procedure.

Introduction

Fiber-reinforced resin composites have received considerable attention in aerospace and astronautics due to their superiority in weight reduction and energy saving.[1–3] Thermosetting resins are the mostly used polymeric matrices for these composites because of their excellent thermal resistance, high stiffness, and high strength.[4,5] Most of the thermosetting resins are obtained by the curing of oligomers in which reactive units can react with each other to form cross-linked polymer networks. The curing behavior is highly complicated as various kinds of reactions are involved in the curing process. For example, various cured structures, such as naphthalene rings, phenyl rings, and polyene structures, can be generated in the curing of arylacetylene resins from the Diels–Alder reaction, cyclotrimerization, and radical polymerization of alkynyl groups.[6–8] As another example, the cured structures of isoindoline, triazine, and phthalocyanine can concurrently be formed *via* the reactions of cyanide units in phthalonitrile resins.[9,10] In principle, the chemical structures of cured polymer networks can be tuned by changing curing conditions, such as curing temperature, curing time, and catalysts. For example, nickel catalysts and Ziegler catalysts are utilized to catalyze acetylene groups to cyclotrimerize in the curing of arylacetylene resins.[11]

Multistep curing strategies, which have a series of combinations of curing temperature and curing time in each step, are commonly used in the curing processes of thermosetting resins, such as epoxy resins, phthalonitrile resins, and arylacetylene resins. The cured structures formed by the reactive units and the properties of the final thermosets are directly related to the curing procedure. Optimizing curing strategies has become an efficient method for preparing high-performance resins with desired properties. For example, Deng *et al.* proposed a curing procedure to enhance the thermal resistance of silicon-containing polyarylacetylene. They found that reducing the curing time at high temperature (above 250 °C) can avoid the oxidation of the Si–CH_3 and alkynyl groups, which can improve the heat-resistance of the cured resin.[12] However, the relationship between the cross-linked structure and the properties of

Shanghai Key Laboratory of Advanced Polymeric Materials, Key Laboratory for Ultrafine Materials of Ministry of Education, Frontiers Science Center for Materiobiology and Dynamic Chemistry, School of Materials Science and Engineering, East China University of Science and Technology, Shanghai 200237, China. E-mail: lq_wang@ecust.edu.cn, jlin@ecust.edu.cn

† Electronic supplementary information (ESI) available. See DOI: 10.1039/d0cp05580h

the cured polymers is still unclear due to the highly complicated nature of the curing behaviors. To date, the optimization of the curing procedure remains trial and error, which is usually based on experimental characterization results.

Theoretical simulation can help to understand the structure–property relationship and accelerate the development of optimized materials. In the theoretical simulation, the research objectives can be easily determined by excluding possible influence factors, which renders it particularly suitable for complicated systems. Molecular dynamics (MD) simulations, one of the most useful theoretical methods, can be adopted to address the fundamental questions arising in the fields of thermosetting resins.[13,14] The thermal and mechanical properties of the polymer networks, such as epoxy resins, have been predicted and compared with those of the experimental results.[15,16] For example, Shenogina *et al.* developed an effective crosslinking approach to construct a set of stress-free molecular models of highly cross-linked epoxy resins.[15] The predicted densities, coefficients of thermal expansion, and glass transition temperatures of the cured epoxy resins are in good agreement with experimental data. Their theoretical methods could be generalized to construct molecular models of other thermosetting polymers. Li *et al.* used MD simulations to predict the network structure and properties of a thermosetting polymer obtained from the curing of diglycidyl ether of bisphenol A (DGEBA) with 3,3′-diamino-diphenyl sulfone (33DDS).[16] The MD simulations quantitatively predicted elastic modulus, coefficient of thermal expansion, and specific heat of the epoxy resin in the glassy state.

Acetylene-terminated polyimides are a kind of commonly used heat-resistant polymers. Compared with the polyimides prepared through a polycondensation reaction, this addition-type polyimides can be processed with a more moderate condition, which is beneficial to the manufacturing of carbon fiber composites. However, there are many drawbacks for the polyimide matrices, such as brittleness and relatively low T_g, which are closely related to the chemical structure and the curing procedure. In the present work, we employed all-atomistic MD simulations to investigate the effect of the curing reaction on the structure and properties of acetylene-terminated polyimides. First, four essential types of reactions in the curing process of acetylene-terminated polyimides were considered, including cyclotrimerization (CT), Diels–Alder reaction (DA), radical polymerizations of three alkynyl groups (RP-3), and radical polymerizations of two alkynyl groups (RP-2), where the former two are cycloadditions and the remainders are non-cycloadditions. At the beginning of this study, we ruled out the interference among these reactions and considered the four reactions independently for the sake of simplification. The crosslinking structures, thermal properties, and mechanical properties of the thermosets obtained from different curing reactions were examined. The results demonstrated the distinction in structures and properties between polymer networks cured with cycloadditions and non-cycloadditions. Finally, curing procedures for real systems (the Diels–Alder reaction, cyclotrimerization, and radical polymerization can take place simultaneously) were designed according to the theoretical studies, and the cured polymers show differences in thermal and mechanical properties. The results can provide a guide for the design of curing procedures to obtain high-performance composites.

Model and simulation

We used all-atomistic MD simulations to study the structure and the properties of cured acetylene-terminated polyimides. The molecular structure of the acetylene-terminated polyimide studied is shown in Fig. 1a. The degree of polymerization of the polyimide can be varied in experiments. In this study, we fixed the degree of polymerization as 1 to show the curing effect of terminated alkynyl units. The curing reaction types of the acetylene-terminated polyimide in its curing process have been studied by gas chromatography-mass spectrometry (GC-MS).[17] The results showed that radical polymerization occurs in the curing process. Two common cycloaddition reactions, that is, cyclotrimerization (CT) and Diels–Alder (DA) reaction, also take place during the curing. These reactions were confirmed in detail using ^{13}C-NMR, solid-state ^{29}Si-NMR, and DFT calculations.[18,19] Herein, we want to understand how the cycloaddition reactions (cyclotrimerization and Diels–Alder reaction) influence the structures and properties of the cured polymer networks. Additionally, the radical polymerizations of three alkynyl groups (RP-3) and two alkynyl groups (RP-2) were also studied to compare with the cycloaddition reactions. Therefore, four types of curing reactions were considered in this study, that is, cyclotrimerization (CT), Diels–Alder reaction (DA), radical polymerizations of three alkynyl groups (RP-3), and radical polymerization of two alkynyl groups (RP-2) (for the detailed reactions, see Fig. 1).

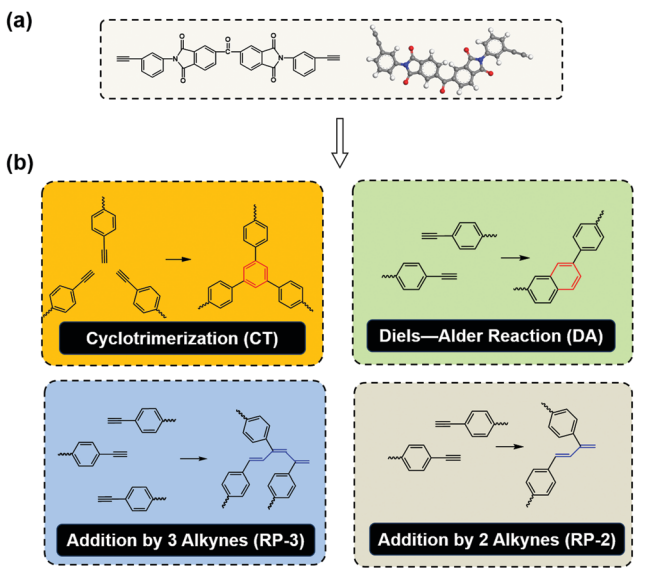

Fig. 1 (a) Targeted acetylene-terminated imide oligomer. (b) Four kinds of curing reactions of alkyne units, including cyclotrimerization (CT), Diels–Alder reaction (DA), radical reactions by three alkynes (RP-3), and radical reactions by two alkynes (RP-2).

Simulation details

A crosslinking approach based on a cut-off distance criterion and a multistep relaxation process was used to build the polymer networks. The crosslinking procedure for polymer networks is similar to the technique widely used for crosslinking thermosetting resins, where new bonds can be created between two reactive sites within the cut-off distance.[20–24]

The procedure for simulating the curing of resins in MD simulations is shown in Fig. S1 (ESI†). The resin molecules are initially randomly distributed in a cubic box with periodic boundary conditions. The simulation was first performed in an *NPT* ensemble at T = 800 K and P = 1 atm for 1 ns to relax the system. Such simulations were performed for five replicas that differ in the initial distribution of the resin molecules within the simulation cell. The distances between reactive groups are then checked for the uncured resins to find the potential sites for reactions. The initial cut-off distances for the reactions are calculated from the root-mean-square distances (RMSDs) of intermolecular pairs of alkynyl groups. Reactive groups that meet the reaction conditions are constrained through a weak harmonic potential. The spring strength is increased, and the equilibrium length is decreased step by step until the parameters of the targeted bond are reached. Afterward, the simulation model is relaxed by structure optimization and *NPT* simulation of 10 ps to avoid high internal stresses and unrealistic geometry distortions. The above procedure is repeated to increase the curing degree of the system. As the extent of reaction increases, the RMSDs between reactive groups are also increased. Therefore, the cut-off distances are accordingly increased to accelerate the curing reaction and reduce the computational time. More information about the crosslinking process can be found in the ESI.†

All the simulations were performed with Materials Studio from Accerlrys Inc.[25] The Forcite module was used to run the MD simulation. The time step was kept at 1.0 fs. The Andersen thermostat and Berendsen barostat were applied to control the temperature and pressure, respectively. The COMPASS force field acted in the whole simulation.[26] van der Waals and Coulomb force were calculated by the atom-based summation method and Edward method, where the cut-off distance is 12.5 Å. Before the calculation of properties, a 100 ns MD simulation was performed to equilibrate the system.

Free volume analysis

The free volume of the polymer network was calculated as follows.[27] The simulation space is binned using a cubic grid, the size of which is smaller than that of the atoms. The total free volume and the distribution of void size can be obtained by counting the volume of a void accessible to a spherical probe with a specific diameter. The accuracy of free volume calculation is sensitive to the bin size and the diameter of the probe. We used the grid size of 0.25 Å and varied the probe size in the free volume calculation.[27]

Calculation of glass transition temperature

Glass transition temperatures T_g were evaluated by cooling the thermosets at a rate of 0.1 K ps^{-1} in an *NPT* ensemble. The density at each temperature was computed by averaging the results from the last 50 ps, and the density–temperature responses were constructed correspondingly. In the cooling process, the dependence of the density on the temperature shows an abrupt change due to the different motion types of the chain segment in the glass state and rubbery state. Such a change is usually used to determine the T_g. Linear fitting was applied to the data in the low- and high-temperature ranges, and the T_g was obtained from the intersection of the two linear fits.

Calculation of mechanical properties

Stress–strain behavior was modeled using a dynamic method described in ref. 28. Compared with the static method, this method takes into account potential energy as well as entropic and vibrational contributions to the mechanical response of thermosets.[28,29] A stepwise deformation method was adopted.[28] The bulk modulus, shear modulus, and Young's modulus (and Poisson's ratio) were obtained by applying isotropic expansion, shear deformation, and uniaxial elongation to the systems, respectively. The deformation rate in all the calculations is 10^8 s^{-1}. At each step, the structure was deformed by 0.1% and then subjected to energy minimization and *NVT* equilibration for 10 ps. For studying each reaction, five simulation models with different initial configurations were used to calculate the mechanical properties. Young's modulus was obtained by applying tension and compression uniaxial strains individually at each coordinate direction of the simulation cell and calculated as $\sigma_{ii}/\varepsilon_{ii}$, where σ_{ii} and ε_{ii} are diagonal elements of the stress and strain tensors, respectively. Bulk modulus was obtained by simultaneously applying equal compression or dilatation strains in all three directions and determined as the initial slope of the curve representing the average of stress tensor diagonal components *vs.* volumetric deformation. Shear modulus was obtained by applying shear deformation in each direction and calculated as $\sigma_{ij}/\varepsilon_{ij}$, where σ_{ij} and ε_{ij} are off-diagonal elements of the stress and strain tensors. Poisson's ratio was obtained in a uniaxial deformation mode. The box sizes of the simulation models were in the range of 40 to 50 Å. Fitting data, collected by deforming the simulation cells up to 1.5%, were averaged over three different directions.

Structural characterization

Local orientational mobility of the phenylene rings (Phs) was calculated both for the rings in the middle of the molecules and the rings connected to the reactive groups. The first-order Legendre polynomial $P_1(t)$ is given by

$$P_1(t) = \langle \mathbf{b}(0)\cdot\mathbf{b}(t)\rangle \quad (1)$$

where $\mathbf{b}(0)$ and $\mathbf{b}(t)$ denote the normal vectors at the beginning (t = 0) and at time t, respectively. The $P_1(t)$ was obtained by averaging over all the rings of five independent samples.

Pair correlation function $g(r)$ was also calculated to characterize the packing structures of cross-linked polymers. The $g(r)$, defined as the probability of finding the molecules separated by

distance r, is expressed as

$$g(r) = \frac{\langle n(r)\rangle}{4\pi r^2 \rho_0 \Delta r} \quad (2)$$

where Δr is a given thickness of the spherical shell, $\langle n(r)\rangle$ is the average molecule number within the shell between r and $r + \Delta r$, and ρ_0 is the entire number density of molecules. It gives a measurement of the spatial organization of molecules around the central molecules and can be used to demonstrate the dispersion and packing state of the unit in the polymer network.

Calculation of order parameter

To measure the ordering of the structures during uniaxial deformation, we introduced an order parameter S to describe the order degree of the molecules. The order parameter S is defined as

$$S = \frac{3\langle \cos^2\theta\rangle - 1}{2} \quad (3)$$

where θ is the angle between the molecule and the tensile direction.

Calculation of dihedral energy curve

The dihedral energy curve was calculated at the B3LYP/6-311G(d,p) level using Gaussian 09.[30]

Results and discussion

In the curing process of acetylene-terminated polyimides, alkynyl groups can undergo Diels–Alder reaction, cyclotrimerization, and radical polymerization.[17,19] The curing structure formed by these reactions was revealed by gas chromatography-mass spectrometry (GC-MS). The conversion of the alkynyl groups of these reactions can be tuned by changing the curing conditions, such as curing temperature and catalysts. In this study, we assumed that the reaction occurs independently in the curing of the acetylene-terminated polyimide. Then, the effect of individual reaction on the structures and properties of cured polymers was examined. Such a study can deepen our understanding of each curing reaction and exclude the influence of other reactions. According to the theoretical analysis, different curing procedures for actual systems in which all the reactions are involved were finally designed, and the properties of the corresponding cured polymers were studied.

Volumetric properties

We first examined the variation of densities of the thermosets as a function of the extent of reactions to understand how curing reaction types influence the packing of polymers. The extent of reaction is defined as the proportion of the reacted alkynyl groups in the total alkynyl groups. The imide monomers were cured by the four types of curing reactions (CT, DA, RP-3 and RP-2), and the number-average molecular weights (M_ns) of the polymers as a function of the extent of reaction are shown in Fig. S4 (ESI†). Fig. 2 shows the plot of the densities as a function of the reaction extent for the resin systems cured

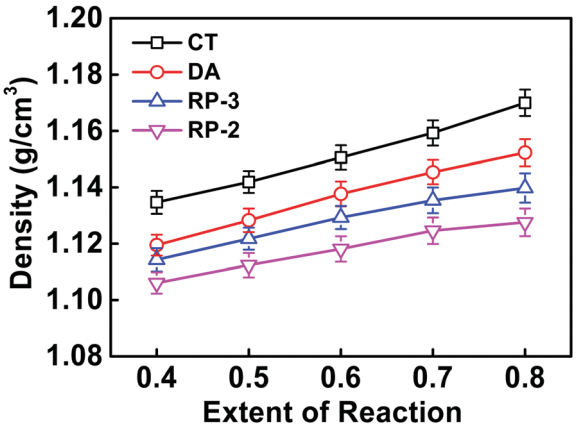

Fig. 2 Density as a function of the extent of reactions for the cured polymer systems. The density was obtained by equilibrating the thermosets with the box size of 41 Å in an *NPT* ensemble (P = 10^{-4} GPa, and T = 800 K) for 1 ns and averaging the data from the last 200 ps.

with different reactions. As shown, a small divergence appears in the density of polymer networks cured *via* different curing reactions. The resins cured by cyclotrimerization (CT) have the highest density, followed by the resins cured by the Diels–Alder (DA) reaction, the radical polymerization of three alkynyl (RT-3), and the radical polymerization of two alkynyl (RP-2). The higher density for cycloaddition (CT and DA) systems is because the formation of aromatic rings can lead to the regular conformation of reacted molecules. Compared with the RP-2, the RP-3 system has a higher density. We analyzed the pair distribution function for molecule pairs in the cured polymers and found that the intermolecular distance in the polymer networks cross-linked by RP-3 is shorter than that in the RP-2 system and is mainly in the range of 4 Å to 6 Å (see Fig. S5, ESI†). This is due to the incorporation of three molecules at each crosslink in the RP-3 system. The shorter intermolecular distance causes a higher density of the RP-3 system.

We further analyzed the free volumes above T_g to gain insight into the density variation for the four cured polymers. The free volume is the volume accessible to a probe with a specific size. The choice of probe size can influence the evaluated free volumes of the polymer networks, where the free volume fractions dramatically decrease with increasing probe size. Fig. 3a shows the free volume fraction for the resins cured with different reaction manners against the probe size. As shown, the free volumes of the four types of cured polymers show similar variation with the probe size. The distribution of pore sizes in the four types of cured systems was further examined using a probe with 0.6 Å. The result is shown in Fig. 3b. One can see that the distribution of void volume in the four cured systems is broader than those in the uncured system. The fraction of small microcavities with a pore size less than 1.5 Å decreases, especially for the structures cross-linked *via* cycloaddition reaction. Meanwhile, holes larger than 3.5 Å appear in the crosslinking structures of the four systems. The cycloaddition systems have microcavities with diameters even larger than 4.5 Å. It has been known that the presence of

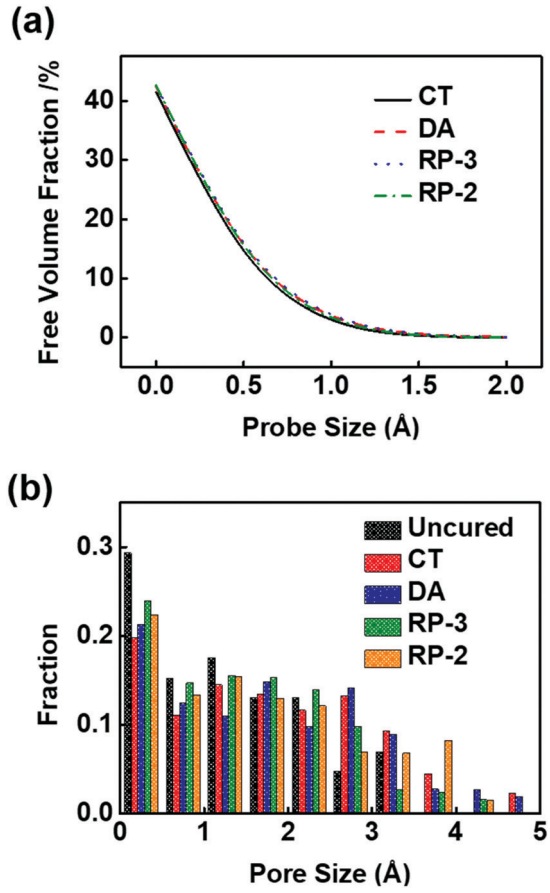

Fig. 3 (a) Free volumes of the cured polymers as a function of probe size. (b) The size distribution of nanovoids for cured polymers with the conversion of 0.8 using the probe with a size of 0.6 Å.

rigid components in polymer networks can increase the size of nanovoids.[31] The curing effect improves the stiffness of the polymers, resulting in a broader distribution of pore sizes.

Energy change and structure evolution during curing

The cured state of each molecule was monitored to get a deep insight into the crosslinking process. There are three states available for a polyimide chain terminated with alkynyl groups, that is, uncured states, one-end cured states, and two-end cured states. Fig. S6 (ESI†) shows the conversion of the resin molecules in each cured state against the extent of reaction.

One can see that four systems with different curing reactions undergo a similar process. At the early stage of the curing process, the monomers are consumed rapidly, while the number of one-end cured molecules increases. As the extent of the reactions exceeds 0.5, the number of one-end cured molecules decreases, and the number of two-end cured molecules increases rapidly.

The change of internal energy for each cured system was analyzed to examine how different kinds of curing reactions influence the structures of cured polymers. In the whole simulation procedure, the total energy of the systems can be described by a COMPASS force field, which consists of bond

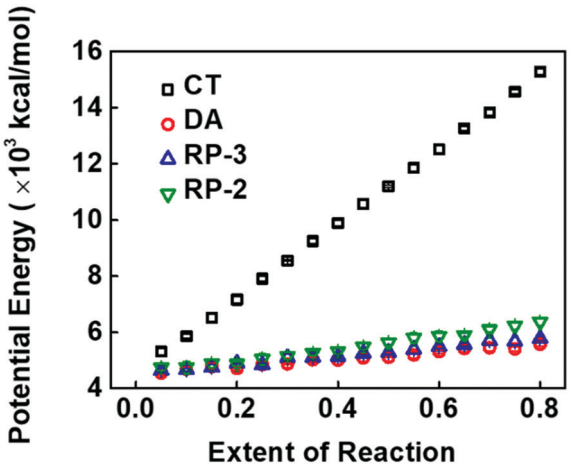

Fig. 4 Variations of potential energy as a function of the extent of reaction. All the energy terms were calculated in a COMPASS force field.

stretches, angle bends, torsion twists, improper torsions, cross terms, and nonbonded interactions (van der Waals and electrostatic interactions). Fig. 4 shows the change of potential energies during the curing for each reaction type. The improper torsion and the cross term are not counted as they contribute little to the total energy. As shown, for the four types of reactions, the potential energies always increase with increasing the conversion, where the potential energies in the system cured with CT increase much more evidently than those in the other three systems.

Among the constituents of potential energies, including the bond energy (Fig. S7a, ESI†), the angle energy (Fig. S7b, ESI†), the torsion energy (Fig. S7c, ESI†), and the nonbonded interaction energy (Fig. S7d, ESI†), the torsion energy plays a dominant role in the increase in total potential energy (see Fig. S7c, ESI†). The torsion energy has been reported to be crucial in the curing process of other resins, such as epoxy resin.[23] During the curing process, the degree of structural restriction increases due to the formation of new bonds, leading to an increase of torsion energy. Among the four curing reactions, the increase in torsion energy for CT is significantly higher than those for other curing types. For the CT, three molecules cyclotrimerize into a rigid benzene ring, which significantly increases the stiffness of the system and the torsion energy.

To examine the role of rigid rings generated from cycloaddition in affecting the structures of cured polymers, we analyzed the geometry of the molecules before and after curing. One of the structural features, the bending angle θ of the molecule, is defined as the angle between the two vectors pointing from the central C-atom to the aromatic C-atoms connected to the imide rings, as shown in Fig. 5a. Because the imide oligomers in this study are constituted by rigid chemical units, the angle defined can reflect the change in the geometry of the whole molecule before and after curing. Analysis of this angle can help understand the effects of cycloadditions on the structures of the cured polymers. Fig. 5b shows

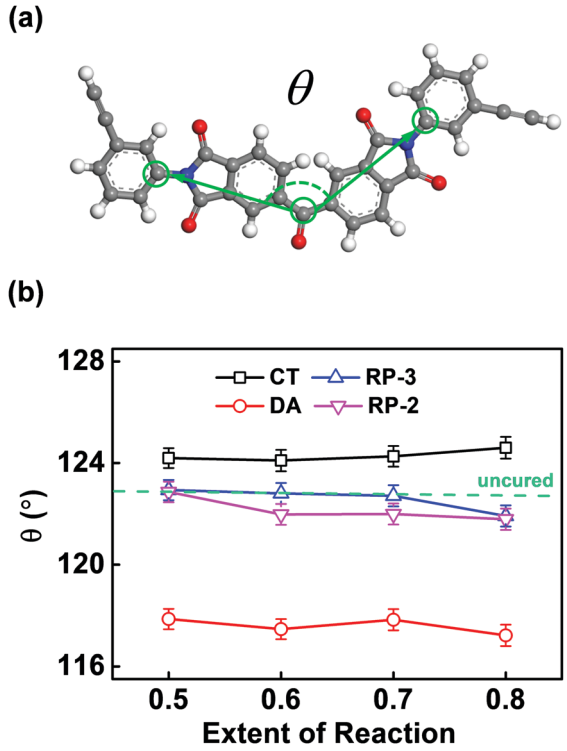

Fig. 5 (a) Bending angle of the monomers created by the atoms colored green. (b) Bending angle of the monomers as a function of the conversion.

the plot of the bending angles of θ as a function of the conversion. As shown, compared with the configuration of uncured resins (dashed line), the molecule cured by CT has a larger θ, which means that the molecule is stretched after the reaction. Meanwhile, the DA reaction exerts a compressing effect on the molecules, resulting in a smaller value of θ. The molecules undergoing radical polymerization have little change as compared with the uncured molecules. The energies of a monomer molecule, under the constraint of various angles of θ, were calculated with the COMPASS force field, and the results are listed in Table 1. It can be seen that either stretching or compressing the molecules causes an increase in energy. The stretched or compressed molecules cannot relax to a more favorable configuration due to the high rigidity of the cycloaddition systems. The results indicate that cycloadditions introduce additional internal stress to the cross-linked systems.

Mechanical and thermal properties of cured polyimides

The mechanical properties of thermosets usually depend upon the curing process of the resins. However, the complicated curing process, involving several crosslinking reactions, makes the structure–property relationship challenging to reveal. Herein, we compared the mechanical properties of cured polymers obtained by different curing reactions. Moduli and Poisson's ratios were calculated for each cured system *via* a dynamic method.

Table 1 Potential energies of monomers with different bending angles

Angle θ (°)	Energy (kcal mol^{-1})
123 (uncured)	−18.21
124 (CT)	−17.50
117 (DA)	−16.68
122 (RP-3, RP-2)	−19.09

Fig. 6 shows the moduli of the resins cured with different reactions *versus* the extent of reactions. The four cured systems behave differently in bulk modulus, shear modulus, Young's modulus, and Poisson's ratio. As shown in Fig. 6a, the cycloaddition (CT and DA) systems have much higher bulk moduli than those of the non-cycloaddition (RP-2 and RP-3) systems, suggesting that the rigid cured structures significantly contribute to the resistance against isotropic compression. By comparing the CT system with the DA system or comparing the RP-3 system with the RP-2 system, it seems that the crosslinking has a less marked effect on the bulk modulus. The shear modulus and Young's modulus for the four cured systems show similar variation as a function of the reaction extent (see Fig. Fig. 6b and c), where the CT system has the highest modulus. The moduli of the resins cross-linked by DA and RP-3 are comparable, while the system cured by RP-2 has the lowest modulus. The results indicate that the rigid cured structures and the crosslinking effect both promote the stiffness of the system. The Poisson's ratio, however, depends upon the topology of the polymers (linear or cross-linked). As shown in Fig. 6d, the linear polymers (DA and RP-2) have higher Poisson's ratios, while the cross-linked systems (CT and RP-3) show lower Poisson's ratios.

We examined the energy variation during uniaxial deformation to further understand the mechanical behaviors of different cured systems. Fig. 7 shows the energy change during the elastic deformation. One can see that in the elastic deformation region of the four cured systems, the nonbonded interaction energy increases significantly, and the other energy terms remain constant as the strain increases. The nonbonded interaction energy plays a dominant role in determining potential energy.

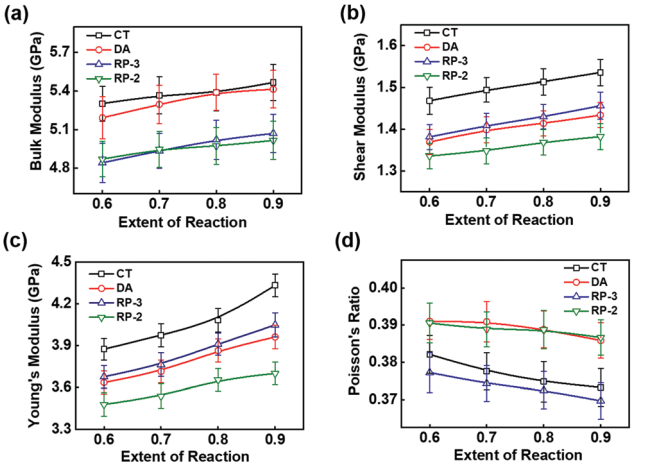

Fig. 6 (a) Bulk modulus, (b) shear modulus, (c) Young's modulus, and (d) Poisson's ratio as a function of the extent of reactions for the four cured polymers at 300 K. The mechanical properties were calculated by the uniaxial elongation with a deformation rate of 10^8 s^{-1}.

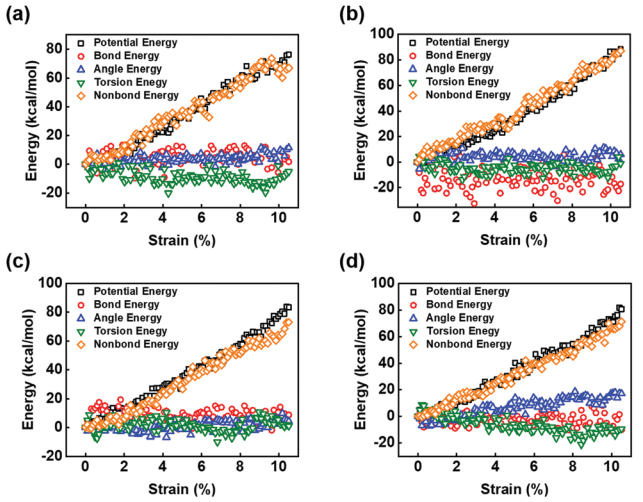

Fig. 7 Energy decomposition under uniaxial deformation for the resins with the reactions of (a) cyclotrimerization (CT), (b) Diels–Alder (DA) reaction, (c) radical reaction by three alkynes (RP-3), and (d) radical reaction by two alkynes (RP-2).

The increase of the nonbonded interaction energy in the elastic deformation region is associated with the small structural adjustment of the chain segment. The results indicate that only local movement is permitted under uniaxial deformation before yielding, which results in high moduli of the four cured systems (see Fig. 6).

The correlation between microstructure and mechanical properties of polymers was further investigated by examining the orientations of monomers during uniaxial deformation for each cured system. The angle in the calculation of order parameter S was defined by crossing the vector of the molecule (created by the aromatic C-atoms connected to the imide rings) and the vector representing the tensile direction (see Fig. 8a). Fig. 8b shows the orientation of the molecules during the uniaxial deformation. As shown, the reacted monomers in the four cured systems are oriented along the deformation direction during the uniaxial elongation. The molecules cured by radical reactions (RP-3 and RP-2) can orient more easily than those cured by cycloaddition (CT and DA), suggesting that the cycloaddition systems exhibit less toughness than the cured systems from radical reactions. The results are in agreement with the experimental observations.[32] In the experiments, the cured polymer in which more polyenes can be formed in the curing process shows high toughness.

The glass transition temperature is crucial for high-performance resins as it determines the temperature range in which the materials can be used as plastics or rubbers. Fig. 9 shows the plots of glass transition temperature as a function of the conversion for all the four cured polymers. As shown, the glass transition temperature increases as the conversion increases. The polymer networks formed by CT and RP-3 have higher T_gs than those of the systems of DA and RP-2. The crosslinking has a pronounced influence on the T_g, while the cycloaddition does not contribute markedly to the increase of T_g. It has been known that the fraction of rotatable bonds and

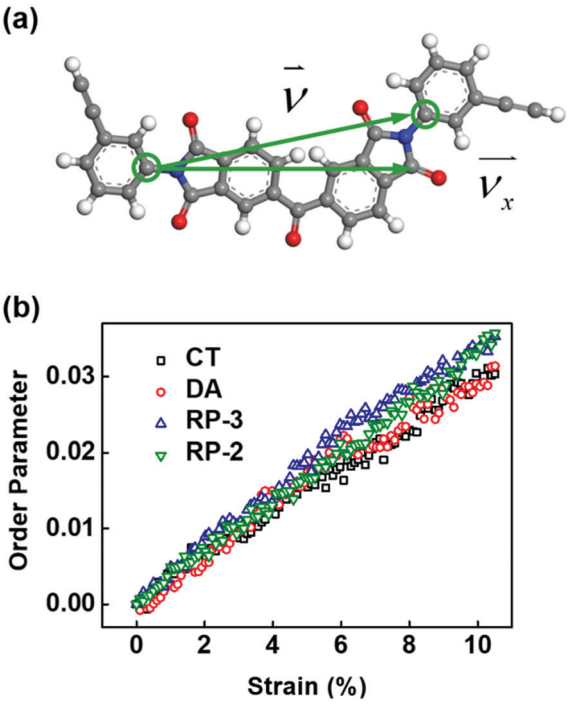

Fig. 8 (a) Definition of the orientation of the monomer. (b) Orientations of the monomers during uniaxial deformation for cured polymer systems. The uniaxial elongation was performed with a deformation rate of 10^8 s^{-1}.

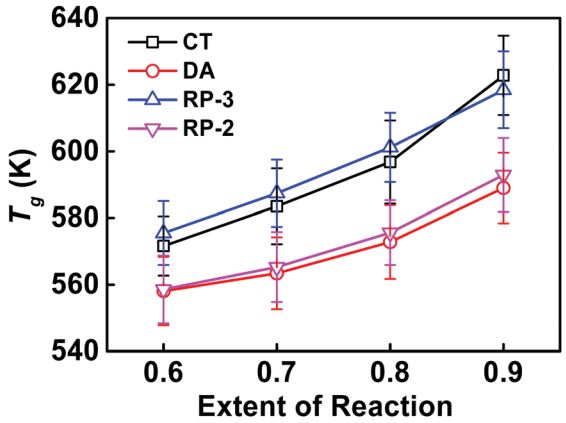

Fig. 9 Glass transition temperature (T_g) as a function of the conversion for the cured polymers under different kinds of reactions.

the fraction of ring atoms are highly correlated with T_g.[33] The ring atoms can increase the stiffness of the polymer and hinder the rotation of the polymer chain. The motion of the chain segment can also be restricted by reducing the rotation ability of the chemical bonds in the backbone. In the polymer systems cured by alkynyl groups, the T_g is increased *via* either increasing the fraction of ring atoms by cycloadditions or restricting the rotation of chemical bonds by radical reactions.

We have compared the calculated T_g with existing experimental values. The acetylene-terminated polyimide with a similar structure has been reported.[34] The DMA measurement shows that this polyimide undergoes glass transition at 314 °C

as DP = 1. According to the WLF equation, the cooling rate shifts T_g towards higher values at a rate of about 3 K per decade. If measured at the same cooling rate as experiments, the calculated T_g values in this study for the cured polymers at the extent of 0.9 should be translated to the range of 300–330 °C. These T_g calculation results are consistent with the experimental observations. These results indicate that our simulations can accurately predict the glass transition temperatures of polyimides.

Segment relaxation and torsion energy curves

The relaxation process was studied to get insight into the effect of curing types on T_g. Fig. 10 shows the relaxation curves of Phs in different positions at 800 K. As can be seen in Fig. 10a, for the Phs in the middle of the molecule, different cured systems exhibit nearly the same relaxation behaviors, indicating that the curing reactions adopted by different systems have a less marked influence on the relaxation process of Phs in the middle. However, the Phs connected to the reactive groups behave in noticeable differences (Fig. 10b). The Phs in RP-3 systems relax the slowest among all cured systems, followed by the Phs in RP-2 systems. The Phs in CT and DA systems show a fast relaxation. The above results indicate that the curing types significantly impact the relaxation process of Phs connected to the reactive groups, which differs from the relaxation of Phs in the middle. Although no ring structures are formed in the systems cured by the radical reaction, the slow relaxation of the Phs shows that the rotation of the polymer chain is also restricted. This leads to the similar T_g values of polymers cured by both cycloadditions and non-cycloadditions with the same degree of polymerization.

Except for the cured structure itself, the connection environment around the Phs, such as the aromatic ring connecting to the aromatic ring in the cycloaddition systems and the vinyl unit connecting to the aromatic ring in the radical reaction system, can also influence the properties of the whole cured systems. We compared the torsion energies of these two kinds of connections by analyzing the torsional potential energy surfaces of the connecting bonds using density functional theory (DFT). The four cured systems have close values of packing densities. Additionally, the intermolecular interaction for the four systems is nearly the same as they are all cured of identical monomers. Therefore, the torsional features (the single-bond torsional potential energy surface) in different cured structures are essentially associated with the torsional properties of the polymers. The results are shown in Fig. 11. As shown, the torsion energy curves of these two connections are different. The rotation of Ph–vinyl is of higher energy barriers and broader energy valleys, while the rotation of Ph–Ph exhibits lower energy barriers and narrower energy valleys. Note that the rotation energy barrier of Ph–vinyl is about 4.41 kcal mol^{-1}, much higher than that of Ph–Ph (2.53 kcal mol^{-1}).

The difference in the torsion energies of Ph–Ph and Ph–vinyl can be used to explain the differences in relaxation behaviors. The difference in torsion energy barriers indicates that the rotation of Ph–vinyl is more complicated than that of Ph–Ph, resulting in the slow rotation relaxation of the Phs connected to

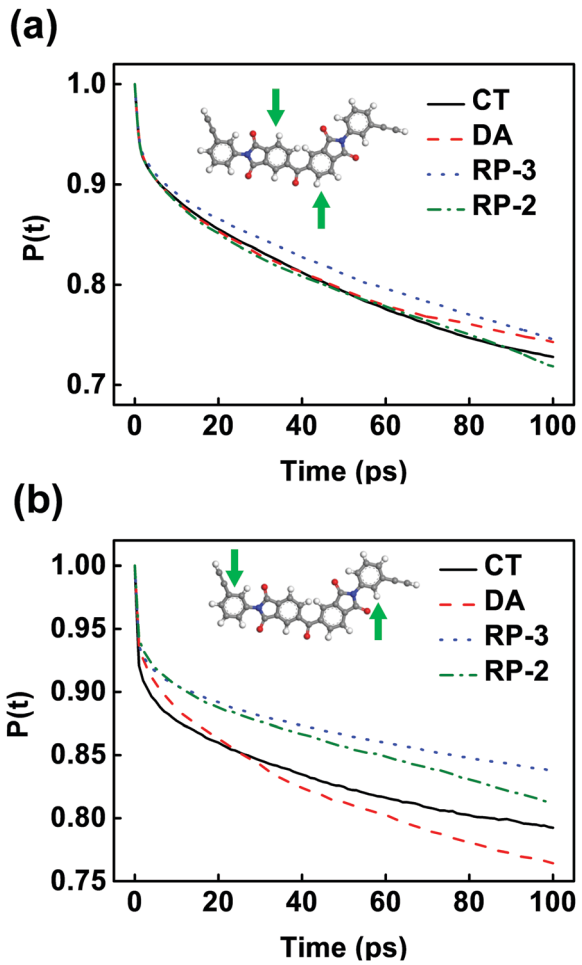

Fig. 10 Relaxation curves of Phs (a) in the middle of the molecules and (b) connected to the reactive groups. The studied Phs are marked with green arrows.

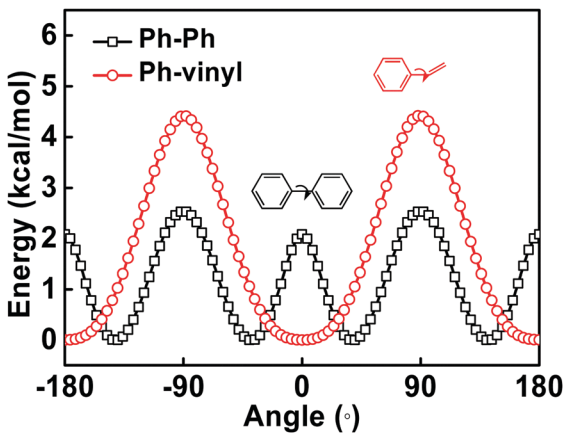

Fig. 11 Plots of the dihedral energies of Ph–Ph and Ph–vinyl as a function of dihedral angles. The dihedral energy curve was calculated with DFT at the B3LYP/6-311G(d,p) level.

the reactive groups in the systems cured by radical polymerization (see Fig. 9). In addition, in the temperature of performing uniaxial elongation, most structures in the system are in the state of the lowest energy. The broad valleys in the curves of torsion energy for Ph–vinyl facilitate the rotation in a small angle range, which results in the high orientation during uniaxial deformation (see Fig. 8b). In contrast, a small configuration change results in a substantial energy increase for Ph–Ph dihedral angle in the energy valley. Consequently, the rotation between Ph and Ph is more restricted, resulting in the low orientation in the cycloaddition systems during uniaxial deformation (see Fig. 8b).

Combined effects of various curing reactions

Higher modulus and toughness are desired as acetylene-terminated polyimides are used as the matrices in carbon fiber composites. The results of Fig. 6 and 8 indicate that cycloadditions promote the bulk modulus and Young's modulus of the cured polymer, and the radical polymerization facilitates the toughness of the cured polymer. Therefore, we designed two cured polyimides to see whether the reaction types play the same role as three types of reactions are combined. The first curing procedure aimed to obtain the cured polyimide with good toughness. The imide oligomers were cured at a low temperature for the total curing process to produce more polyenes. The second procedure aimed to obtain the cured polyimide with a high modulus. The imide oligomers were cured first at a low temperature and then at a high temperature. The curing at a low temperature is needed to avoid explosive polymerization. More alkynyl groups can undergo cycloadditions in the second curing procedure. The product cured by the first curing procedure is composed of 75 wt% polyenes, 20 wt% triphenylbenzenes, and 5 wt% phenylnapthalenes. The product cured by the second curing procedure is composed of 60 wt% polyenes, 30 wt% triphenylbenzenes, and 10 wt% phenylnapthalenes. The details of simulation methods for these two curing procedures can be found in Section S6 of the ESI.† These two curing procedures can be easily realized in experiments.

We then studied the thermal and mechanical properties of the two cross-linked polyimides cured by these two curing procedures. It was found that the glass transition temperatures T_g of the two cured polyimides are 585.2 K and 587.8 K for curing procedure-1 and curing procedure-2, respectively. The T_g does not show a distinct difference in these two cured polymers cured by different curing procedures because the cycloadditions and non-cycloadditions of the alkynyl groups have similar effects of restricting the chain segments. As discussed before, both the increased fraction of ring atoms formed by the cycloadditions and the decreased fraction of rotatable bonds caused by radical polymerization can hinder the motion of chain segments (see Fig. 9–11). Table 2 shows that the polymer cured by the second procedure shows higher moduli (bulk modulus, shear modulus, and Young's modulus) and lower Poisson's ratios compared with those of the polymer cured by the first procedure. This is because cycloadditions in the high curing temperature can lead to the formation of more rigid rings. As can be seen in Fig. 6, the systems cured by cycloadditions show strong abilities to resist deformation and have high moduli.

Table 2 Bulk modulus, shear modulus, Young's modulus, and Poisson's ratio of the polymers cured by different curing procedures

Curing procedure	Bulk modulus (GPa)	Shear modulus (GPa)	Young's modulus (GPa)	Poisson's ratio
1	4.99 ± 0.13	1.39 ± 0.02	3.82 ± 0.08	0.3820 ± 0.0047
2	5.18 ± 0.16	1.43 ± 0.03	4.09 ± 0.09	0.3719 ± 0.0051

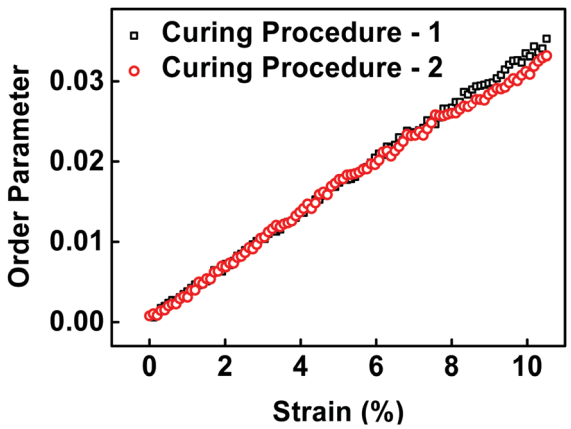

Fig. 12 Orientations of the monomers during uniaxial deformation for polymers cured by different curing procedures.

Fig. 12 shows the orientation of the molecules in the two cured systems during the uniaxial deformation. The polyimides cured by the first curing procedure can orient more easily than those cured by the second curing procedure, suggesting that the first curing procedure can promote the toughness of the polymers. As illustrated in Fig. 8 and 11, the formation of polyenes can facilitate the structural adjustment (such as the rotation in a small angle range) during elongation and improve the toughness.

The above analysis indicates that changing the curing procedures such as curing temperature and curing time can tune the degrees of curing reactions and optimize the properties of the thermosetting polymers by producing different polymer networks. Based on the relationships between cured structures and properties obtained in this study, we can optimize the curing procedures to obtain thermosetting polymers with desired thermal and mechanical properties, such as glass transition temperature, modulus, and toughness. Additionally, we can predict the properties of the resins before experiments to avoid trial and error, which is an easy and efficient way to prepare high-performance resins.

Conclusions

We performed all-atomistic MD simulations to study the structures and properties of imide oligomers cured with different

reactions between alkynyl groups. To obtain reasonable cured structures within a feasible computational time, we used a crosslinking approach based on a cut-off distance criterion and a multistep relaxation process. The effects of curing reaction types on the structures and properties of cured polymers were investigated. The mechanical properties of the cured polyimides, including bulk modulus, shear modulus, Young's modulus, Poisson's ratio, and toughness, show significant differences as the curing reaction types are changed. The toughness can be enhanced by RP reactions due to the quick orientation of molecules in such a system, while the bulk modulus can be increased by CT and DA reactions because of the formation of rigid cured structures. Moreover, the crosslinking reactions from CT and RP-3 can improve the shear and Young's moduli of the thermosets ascribed to the highly branched structures. We found that different curing reaction types lead to the increase in glass transition temperatures of the polymers in different ways. The CT and RP-3 can generate local branched structures, restricting the rotation of neighboring bonds and leading to higher glass transition temperatures than those of the systems cured by DA and RP-2. The knowledge obtained from this study can be used for optimizing the curing process to prepare high-performance materials with desired properties. Due to the limiting time scale involved in all-atom MD simulations and the limitation of the crosslinking method, thorough understanding of the curing kinetics and the properties related to the curing time of acetylene-terminated polyimides is hindered. A multiscale simulation method has to be developed in the future to gain deep insight into such subjects.

Conflicts of interest

There are no conflicts to declare.

Acknowledgements

This work was supported by the National Natural Science Foundation of China (51833003, 21975073, and 51621002).

Notes and references

1 P. K. Mallick, *Fiber-reinforced composites: materials, manufacturing, and design*, CRC Press, 3rd edn, 2008.
2 I. D. Robertson, M. Yourdkhani, P. J. Centellas, J. E. Aw, D. G. Ivanoff, E. Goli, E. M. Lloyd, L. M. Dean, N. R. Sottos, P. H. Geubelle, J. S. Moore and S. R. White, *Nature*, 2018, **557**, 223–227.
3 N. V. Handa, S. Li, J. A. Gerbec, N. Sumitani, C. J. Hawker and D. Klinger, *J. Am. Chem. Soc.*, 2016, **138**, 6400–6403.
4 Q. Guo, *Thermosets: structure, properties and applications*, Woodhead Publishing, 1st edn, 2012.
5 T. Kaiser, *Prog. Polym. Sci.*, 1989, **14**, 373–450.
6 S. Gandon, P. Mison, M. Bartholin, R. Mercier, B. Sillion, E. Geneve, P. Grenier and M. F. Grenier-Loustalot, *Polymer*, 1997, **38**, 1439–1447.
7 S. Gandon, P. Mison and B. Sillion, *Polymer*, 1997, **38**, 1449–1459.
8 K. Guo, P. Li, Y. Zhu, F. Wang and H. Qi, *Polym. Degrad. Stab.*, 2016, **131**, 98–105.
9 T. M. Keller and D. D. Dominguez, *Polymer*, 2005, **46**, 4614–4618.
10 M. Laskoski, D. D. Dominguez and T. M. Keller, *Polymer*, 2007, **48**, 6234–6240.
11 S. Pasynkiewicz, E. Olędzka and A. Pietrzykowski, *Appl. Organomet. Chem.*, 2004, **18**, 583–588.
12 X. You, S. Deng, Y. Huang, Z. Liu and Y. Hu, *J. Appl. Polym. Sci.*, 2019, **136**, 47301.
13 J. D. Monk, J. B. Haskins, C. W. Bauschlicher and J. W. Lawson, *Polymer*, 2015, **62**, 39–49.
14 J. Kang, C. Wang, D. Li, G. He and H. Tan, *Phys. Chem. Chem. Phys.*, 2015, **17**, 16519–16524.
15 N. B. Shenogina, M. Tsige, S. S. Patnaik and S. M. Mukhopadhyay, *Macromolecules*, 2012, **45**, 5307–5315.
16 C. Li, G. A. Medvedev, E.-W. Lee, J. Kim, J. M. Caruthers and A. Strachan, *Polymer*, 2012, **53**, 4222–4230.
17 G. Gao, S. Zhang, L. Wang, J. Lin, H. Qi, J. Zhu, L. Du and M. Chu, *ACS Appl. Mater. Interfaces*, 2020, **12**, 27587–27597.
18 M. Itoh, K. Inoue, K. Iwata, M. Mitsuzuka and T. Kakigano, *Macromolecules*, 1997, **30**, 694–701.
19 Z. Chen, L. Wang, J. Lin and L. Du, *Phys. Chem. Chem. Phys.*, 2020, **22**, 6468–6477.
20 J. Zhu, M. Chu, Z. Chen, L. Wang, J. Lin and L. Du, *Chem. Mater.*, 2020, **32**, 4527–4535.
21 L. Gao, Q. Zhang, H. Li, S. Yu, W. Zhong, G. Sui and X. Yang, *Polym. Chem.*, 2017, **8**, 2016–2027.
22 F. K. Schwab and C. Denniston, *Polym. Chem.*, 2019, **10**, 4413–4427.
23 C. Li and A. Strachan, *Polymer*, 2010, **51**, 6058–6070.
24 E. Zhou, L. Wang, J. Lin, J. Zhu, L. Du, S. Deng, J. Gu and L. Zhang, *Acta Polym. Sin.*, 2019, **50**, 1322–1330.
25 Accelrys Software Inc., Materials Studio, http://accelrys.com/products/materials-studio/.
26 H. Sun, *J. Phys. Chem. B*, 1998, **102**, 7338–7364.
27 C. Li and A. Strachan, *Polymer*, 2016, **97**, 456–464.
28 N. B. Shenogina, M. Tsige, S. S. Patnaik and S. M. Mukhopadhyay, *Polymer*, 2013, **54**, 3370–3376.
29 D. N. Theodorou and U. W. Suter, *Macromolecules*, 1986, **19**, 139–154.
30 M. J. Frisch, G. W. Trucks, H. B. Schlegel, G. E. Scuseria, M. A. Robb, J. R. Cheeseman, G. Scalmani, V. Barone, B. Mennucci and G. A. Petersson, *et al.*, *Gaussian 09, Revision A.02*, Gaussian, Wallingford, CT, 2009.
31 R. M. Elder, D. B. Knorr, J. W. Andzelm, J. L. Lenhart and T. W. Sirk, *Soft Matter*, 2016, **12**, 4418–4434.
32 P. M. Hergenrother, *J. Macromol. Sci., Part A: Pure Appl. Chem.*, 1980, **19**, 1–34.
33 C. Kim, A. Chandrasekaran, T. D. Huan, D. Das and R. Ramprasad, *J. Phys. Chem. C*, 2018, **122**, 17575–17585.
34 A. O. Hanky and T. L. St Clair, *Int. J. Adhes. Adhes.*, 1983, **3**, 181–187.

